Journal of Advanced Joining Processes 9 (2024) 100193

Contents lists available at ScienceDirect

Journal of Advanced Joining Processes

journal homepage: www.sciencedirect.com/journal/journal-of-advanced-joining-processes

In situ EDXRD measurement of the low transformation temperature effect in laser beam welded stainless steel

F Akyel [a,*], M Gamerdinger [a], K Mäde [a], K.R.Krishna Murthy [a], S. Olschok [a], R. Sharma [a], U. Reisgen [a], G. Abreu-Faria [b], G. Dovzhenko [b]

[a] *RWTH Aachen University Welding and Joining Institute, Pontstrasse 49, 52062 Aachen, Germany*
[b] *Helmholtz Centre Hereon, Institute of Materials Physics, Max-Planck-Straße 1, 21502 Geesthacht, Germany*

ARTICLE INFO

Keywords:
Laser beam welding
Dissimilar welding
EDXRD
In situ strain measurement
LTT
Phase transformation

ABSTRACT

This paper investigates the low-transformation-temperature (LTT) effect in austenitic high alloy stainless steel and its influence on strain evolution of laser beam welded specimen. Due to the local heat input high temperature gradients occur between weld seam and base material, which lead to thermal and transformation induced strains. With targeted alloying in the weld seam the martensitic phase transformation can be shifted to lower temperatures resulting in the so-called Low Transformation Temperature (LTT) effect. This effect uses the volume expansion during the martensitic phase transformation. The delayed volume expansion during martensite phase transformation introduces continuous compressive strains until room temperature is reached and represents a mechanism that can serve to counteract the tensile strains caused by thermal shrinkage. The martensitic microstructure is achieved by dissimilar welding, combining an austenitic stainless steel base material with low alloyed filler wire. With this, the chemical composition of chromium and nickel is diluted, and a martensitic phase transformation occurs. As comparison, similar material combinations of stainless steel base material and conventional welding consumable are performed. In this work, *in situ* energy-dispersive x-ray diffraction (EDXRD) measurements in the beamline P61A at DESY are performed to investigate the expansion behaviour of martensite based on spectral data. Nine measuring positions are recorded and the strain evolution during welding and cooling of the samples are analysed. It is shown that the martensitic phase transformation changes the strain behaviour and implements compressive strain depending on the distance to the laser spot. It is found that the effect is orientation-dependent and that the highest strain influence is present in welding direction.

Introduction

The local heat input of a welding process influences the thermo-mechanical properties. The inhomogeneous heat distribution leads to zones of different thermal expansion and shrinkage, which in turn promotes residual stresses and distortion (Withers et al., 2001). While residual stresses reduce component load capacity, distortion leads to a decrease in geometric precision (Francis et al., 2008; Francis et al., 2007). Since residual stresses have a relevant influence on fatigue strength, they should be avoided as much as possible to maintain fatigue resistance (Klassen et al., 2017).

It is known that compressive stresses are generated during phase transformations. The authors Jones and Alberry (Jones et al., 1977) suggested as early as 1977 that the strains associated with the transformation of martensite can be used to develop welded joints that reduce tensile residual stresses and avoid post weld heat treatment. This exploits the effect that a face-centred cubic unit cell has a smaller volume than a tetragonally distorted lattice such as martensite (Bhadeshia, 2002; Bhadeshia and Honeycombe, 2017). Especially when delaying the martensite transformation temperature by means of chemical composition, the volume expansion increases. This so called low-transformation temperature effect (LTT-effect) has been successfully used in recent years to counteract the tensile residual stress due to thermal shrinkage (Igwemezie et al., 2022; Francis et al., 2008; Azizpour et al., 2019).

It should be noted that during the phase transformation the thermal shrinkage continues, thus implementing tensile stresses. However, the tensile residual stress in a weld can be compensated if the phase transformation takes place at reduced temperatures and continues until room temperature is reached. Only this way can compressive stress be built up continuously and tensile stress be reduced. Therefore, the LTT-effect is

* Corresponding author.
E-mail address: akyel@isf.rwth-aachen.de (F. Akyel).

https://doi.org/10.1016/j.jajp.2024.100193

Available online 24 January 2024

used to exploit this advantage by means of variation in chemical composition in order to adjust the martensite formation temperature. Furthermore, distortion can be reduced. Overall, an exceeding of the temperature-dependent yield strength can be prevented and plastic distortion can be reduced (Withers et al., 2001; Mikami et al., 2009). As a result, with changes to the chemical composition it is possible to not only reduce residual stress, but also the distortion at the same time.

Austenitic stainless steel is a material prone to warpage, so it is of interest to investigate the use of the LTT-effect in this material. Mostly, it is important to understand, how the strains occurring during phase transformations effect the overall strain distribution in a sample. EDXRD measurements during welding and cooling of a sample are performed on dissimilar welded materials. The change in chemical composition during a laser beam welding process recreates the LTT-effect, while similar welds are used to have a comparison to commonly performed welding trials.

State of the art

Residual stresses are a result of local discrepancies in a material through mechanical or thermal influences or caused by phase transformations (Withers et al., 2001; Wohlfahrt, 1986). The local heat input causes high temperature gradients compared to the areas further away from the weld zone. The increased thermal expansion of the weld zone is restricted by the cooler surrounding area with less thermal expansion. During welding this leads to compression. After the heat input is finished, the weld zone starts to shrink, which in turn leads to tensile stresses, Fig. 1.

Areas where phase transformation occurs contribute to the implementation of stresses due to their different coefficients of thermal expansion, (Mitter, 1987; Bühler et al., 1933). Residual stresses are thus a superposition of stresses resulting from thermal shrinkage as well as phase transformations. A γ-α phase transformation that takes place during cooling has a higher volumetric expansion than the reverse transformation during the heating phase and compressive stresses are generated during the cooling phase. Often, however, these compressive stresses are not sufficient to compensate for the tensile stresses caused by shrinkage, overall resulting in tensile residual stresses in the weld at the end of the process. However, studies have shown that martensitic phase transformation can implement compressive stresses that compensate for tensile stresses depending on the chemical composition (Akyel et al., 2022b; Akyel et al., 2022a).

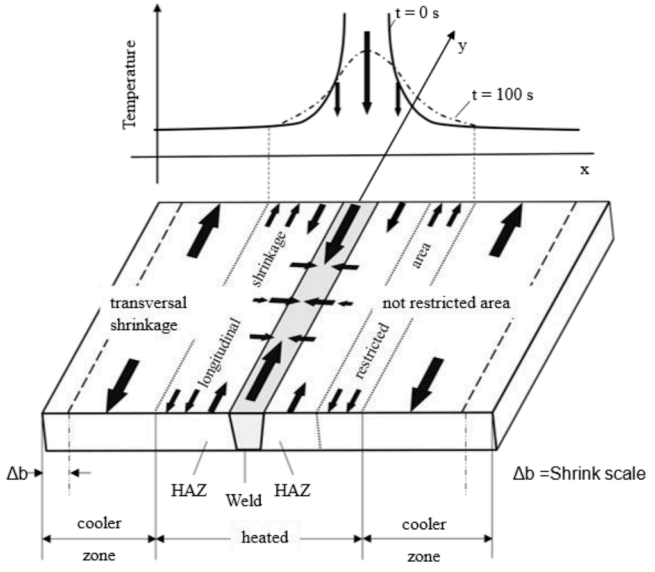

Fig. 1. Single pass weld and its resulting stress distribution (Wohlfahrt et al., 1977).

Achieving a martensitic structure in a weld metal within an optimum temperature range depends mainly on the composition of the filler metal. Chromium in particular leads to an increase in volume change. Increased nickel content also leads to an increase in volume change, although the influence is not as strong as for chromium. For example, 2 m % chromium leads to a relative volume change from austenite to martensite of 0.5 %. In contrast, slightly above 2 m % nickel leads to a relative volume change of just under 0.4 %. (Bleck, 2016)

Therefore, the examination of an austenitic stainless steel is advantageous, since high amounts of chromium and nickel are already present. Through dissimilar welding with low-alloy filler metal, the element content can be reduced in the weld to a range where martensite is formed.

Based on the work of Jones in 1977, many investigations on LTT filler metals have been carried out (Jones et al., 1977). The most notable breakthrough was made by a group of researchers lead by Ohta from Japan with the design of a filler metal containing 10 % chromium and 10 % nickel, which improved the fatigue strength of the welded joint in a low-carbon steel (Ohta et al., 2003; Ohta et al., 2001; Ohta et al., 1999). However, due to the low spatial resolution, residual compressive stresses in the weld could not yet be detected.

Wang, Huo et al. performed investigations with varying chromium and nickel contents (Wang et al., 2002). These confirmed the increase in fatigue strength observed by Ohta. The work also established a first correlation between the compressive residual stresses and the martensite start temperature.

Kromm et al. investigated the transformation behaviour of different chromium-nickel alloy compositions (Kromm et al., 2011; Kromm and Böllinghaus, 2011). Using in-situ diffraction experiments, the research group was able to demonstrate that the high compressive residual stresses are generated only by the martensite phase. These investigations were also confirmed by Altenkirch et al. (2011), Gibmeier et al.(2014).

Energy dispersive X-ray diffraction (EDXRD) experiments are performed to obtain information about the microstructure and the phases in a material from the characteristic X-rays and the energy level detected from them. The development of this measurement method dates to late 1960 early 1970 and was depicted as a novel measurement method in contrast to the angular dispersive measurement methods, (Laine et al., 1980; Giessen et al., 1968). While the scattering angle 2θ is fixed, the sample is irradiated with a polychromatic synchrotron radiation. This measurement method provides both a complete diffraction spectrum and the interference lines of all crystalline phases of the material structure. Using Eq. (1)

$$E_{hkl} = \frac{h * c}{2 * d_{hkl} * \sin\theta} = \frac{h * c * \sqrt{h^2 + k^2 + l^2}}{2 * a_{hkl} * \sin\theta} \quad (1)$$

the energy level E_{hkl} of the centre position of a peak is used to calculate the lattice specific unit cell parameter a_{hkl}, with the constants of the speed of light $c = 299{,}792{,}458$ m/s and Planck's constant h = 4.135*10^(-15) eVs. An angle-dependent measurement or tilting of the sample to capture all orientations is not necessary. With the further development of high-brilliance synchrotron sources, the EDXRD measurement results in a fast measurement method with acquisition rates in seconds (Jenkins and Snyder, 1996; Spieß et al., 2009).

Experimental

Materials and methods

For the welding trials an austenitic stainless steel base material (1.4301/AISI 304) with the dimensions 8 × 50 × 600 mm^3 (width x height x length) is used. A single pass bead on plate is welded along the middle of the 8 mm side. Furthermore, a rectangular seam preparation is used with the dimensions 1.6 × 1.5 mm^2 width and depth respectively, Fig. 2.

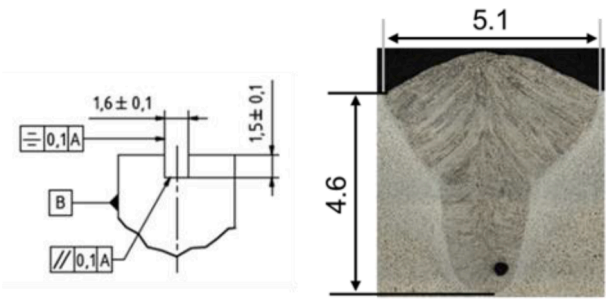

Fig. 2. Seam preparation for the similar and dissimilar welding trials as well as the resulting weld geometry.

To use the LTT-effect, a martensitic microstructure needs to be present. Since the martensite formation is dependent on the chemical composition, the chromium and nickel contents within the weld seam needs to be reduced. Accordingly, this is achieved by the use of a dissimilar material to the base material. The dissimilar welds are performed with the solid filler wire G 3Si1 (EN ISO 14341-A: G 3Si1/ AWS A5:18: ER70S-6). As comparison, similar welds with the solid filler wire G19 9 (EN ISO 14341-A G19 9 L Si/ AWS A5.9: ER308LSi) are performed. All wires have a diameter of 1 mm. For chemical composition analysis, the filler wires are melted in a melting furnace under argon atmosphere and measured with optical emission spectroscopy (OES). Furthermore, the average chemical composition of the weld is analysed by energy dispersive X-ray spectroscopy (EDS) line scans, Table 1.

Welding trials are carried out on a TRUMPF TruDisk 8001 disc laser, which has a maximum beam power of 8 kW at 1030 nm wavelength. The used fibre has a diameter of 400 µm. With an aspect ratio of 3:1 of the optic, the focal diameter is 1200 µm. This diameter in combination with beam oscillation is used to melt the 1 mm cold filler wire and parts of the base material, so that intermixing of both materials creates a defined chemical composition in the weld seam. The inclination angle of the filler wire is 45 ° using the MiniDrive feeding system developed by the RWTH Aachen University Welding and Joining Institute. The inclination points towards the weld bead (pull technique). The shielding gas nozzle is coaxial to the filler wire and 25 ln/min (litre normal per minute) Argon (DIN EN ISO 14175: I1) is used in all trials, Table 2.

The wire feed speeds for the similar and dissimilar welds are set as 4.5 m/min. Temperature measurements in pre trials and a simulation of thermal distribution is used to calculate the temperature distribution over the complete sample.

Energy-dispersive X-ray diffraction

EDXRD measurements are carried out at a synchrotron beamline P61A at the Deutsche Elektronen Synchrotron (DESY) in Hamburg. Acquisition is performed by two high-purity germanium point detectors, each with two slit collimators that can be independently positioned horizontally and vertically. The photon source are 10 wigglers with a polychromatic energy bandwidth between 30 – 200 keV. The data is calculated with an in-house software and the peak fit is performed with a Pseudo-Voigt approximation, Table 3.

Detector 0 (channel 0) measures horizontal reflections and is aligned with the incident beam at an angle of $2\theta_{Ch0} = 7.557$ ° Detector 1 (channel 1) measures in the vertical plane and is oriented at an angle of $2\theta_{Ch1} = 7.594$ ° The slit collimators in front of the horizontal channel have a horizontal slit spacing of 0.1 mm. The collimators in front of the vertical channel also have a vertical slit spacing of 0.1 mm. The incident beam has a diameter of 0.1 mm. With the arrangement of the detectors and the incident beam diameter, the result is a diamond shaped measurement field of a height of 0.1 mm and a length of 2.069 mm for channel 0 and 2.072 mm for channel 1, Fig. 3. Measurements are taken in transmission mode with a recording rate of 1 Hz. The gauge volume was set exactly in the middle of the sample (4 mm depth) and only the distance to the laser or the weld surface was changed between each welding trial.

Welding trials

When performing the welding experiments and simultaneous synchrotron recording, two time periods are considered. During the welding process, the positions of the laser and the synchrotron radiation are fixed. Only the sample is moved linearly. Since the distance between the measurement point and the laser remains constant the temperature is isothermal. This time period is considered as a steady-state measurement. The welding process lasts for about 37 s. With a recording rate of 1 Hz the synchrotron data of the first 37 time steps are the data of the steady-state measurement. As soon as the welding process is finished, the cooling process starts. The laser switches off, but the recording of the synchrotron data continues. Since the cooling curve of the temperature data is now being recorded, this time period is a transient measurement, Fig. 4. One entire welding process including cooling lasts 500 s.

One specimen is welded for each individual measuring point. After a weld is finished, the setup is moved so that the distance to the laser changes. Here, the distance is varied between -20 mm, -25 mm and -50 mm in y-direction and between 2.5 mm, 4 mm and 8 mm in z-direction.

Data analysis

To investigate the temperature-dependent transformation kinetics the temperature distribution is determined by means of simulation and the temperature measurements by thermocouples. The energy for the centre peak positions E_{hkl} is converted to the lattice specific unit cell parameter a_{hkl} using Eq. (1).

For the calculation of the elastic lattice strain Eq. (2) is used.

$$\varepsilon_{el} = \frac{a_{hkl}(T) - a_0(T)}{a_0(T)} \tag{2}$$

For this calculation the temperature dependent stress-free unit cell parameter $a_0(T)$ has to be known for the α- and the γ-phase. The calculation of the temperature dependent data is done by using the coefficient of thermal expansion α_{th} (CTE). Dilatometry of the weld material as well as the base material is performed and the CTE values for the α- and the γ-phase are measured. CTE was measured as $\alpha_{th,\alpha} = 8.836\times10\text{ˆ}{-6}$/K for the α-phase and $\alpha_{th,\gamma} = 24.261*10\text{ˆ}{-6}$/K for the γ-phase. With the use of Eqs. (2) and (3)

$$\varepsilon_{el} = \alpha_{th} * \Delta T \tag{3}$$

Table 1
Chemical composition of the experimental material and the resulting weld compositions using OES and EDS analysis.

Material	Fe	C	Si	Mn	Cr	Ni	Mo	Cr_{eq}*	Ni_{eq}**
1.4301	70.0	0.03	0.31	1.70	18.38	8.01	0.40	19.45	9.76
G19 9	67.6	0.02	0.76	1.61	19.61	9.68	0.17	20.93	10.91
Purus 42	97.4	0.08	0.93	1.35	0.02	0.02	<0.005	1.40	3,09
Weld (LTT)	81.03	0.03	0.49	1.45	11.72	5.0	0.33	12,78	6,59

* Cr_{eq} = %Cr + %Mo + 1.5*%Si + 0.5*%Nb.
** Ni_{eq} = %Ni + 30*%C + 0.5*%Mn.

Table 2
Welding parameters for the dissimilar (LTT) as well as similar welding trials.

Material	Power P [kW]	Weld speed v_s [m/min]	Wire feed speed v_w [m/min]	Shielding gas flow [ln/min]	Oscillation figure [-]	Amplitude [mm]	Frequency [Hz]
G19 9/ G 3Si1	5	0.8	4.5	25	sine	2	180

Table 3
Data overview on the synchrotron beam source, detectors, and evaluation method.

Source P61A @DESY			
Photon source	**Energy range**	**Incident beam diameter**	**Spectrum**
Wiggler	30 – 200 keV	0.1 mm	White
Detection			
Detectors	**Measuring mode**	**Diffraction angle**	**Recording rate**
Ge-Point detector + slit collimators	Transmission	Channel 0: 7.557 ° Channel 1: 7.594 °	1 s/Spectrum
Evaluation			
Diffraction lines	**Lattice parameters**	**Peakfit**	**Software**
bcc: 211 fcc: 311	bcc: 2,8884 Å fcc: 3.5911 Å	Pseudo-Voigt	DESY in-house

and the knowledge of the temperature distribution as well as the CTE, the temperature dependent stress-free unit cell parameter $a_0(T)$ is calculated, Eq. (4).

$$a_0(T) = a_0(T_0) * (1 + \alpha_{th} * (T - T_0)) \quad (4)$$

All these calculations are performed after the peak positions are determined. The 8 mm thick sample together with the background noise and the acquisition rate of 1 Hz leads to some reflections having low peak intensities and partly disappearing in the background, Fig. 5. The peak fitting with the Pseudo-Voigt approximation is only applied for the γ-phase {311} as well as for the α-phase {211} diffraction lines as these lines distinguish themselves clearly from the background.

For each individual time step, the peaks are fitted and plotted over the complete 500 s welding process, Fig. 6. After tracking the peak progression over time, the shift in the energy level can be used to calculate the change in the lattice parameters. Both, the changes during welding and cooling can be displayed and phase transformations recorded. This analysis is repeated for both channels.

Results and discussion

The EDXRD measurements reveal differences in the phase transformations of the two material combinations. Fig. 7 shows the change of the peak positions in channel 0 at measuring point $z = 4$ mm and $y = -20$ mm. The result of the similar welding shows only austenite in the weld seam. A bcc phase does not seem to be present, or the signal is so low that it disappears in the background noise and cannot be detected. Only fcc phase can be detected. In the case of the dissimilar weld, on the other hand, bcc-phase first appears after 172 s which equals to a temperature of around 180 °C. Dilatometric measurements of the weld composition showed a martensite start temperature of around 220 °C.

In the steady-state process, a change in peak positions is measured. Although the temperature at the measuring point is constant during welding, the plotted peak history records a shift in energy range. The shift represents a spatial resolution of the lattice parameter over the weld length. It is known that the peak position is affected by lattice distortion (Genzel et al., 2011). Looking at Eq. (1), it becomes clear what a shift in energy level means. While the energy increases, the interplanar d_{hkl}-spacing or the lattice parameter a_{hkl} reduces. This results in local shrinkage, especially in the middle sections of the weld length, which are cancelled out by pronounced expansion towards the end of the sample. Once the welding stops and the cooling process starts the centre of the peak positions shift to higher energy levels again. Due to the cooling, continuous shrinkage occurs explaining the peaks shift to higher energy levels.

After each individual specimens or measuring points have been evaluated, the strains are calculated according to Eq. (2). The distances to the laser at -20 mm, -25 mm and -50 mm are compared. The diagrams are also divided according to the distances to the component surface at 2.5 mm, 4 mm, and 8 mm and according to the recording channels horizontal channel 0 and vertical channel 1.

For the strain calculation the stress-free lattice parameter needs to be known. During the trials it was not possible to measure this value since the chemical composition for achieving the LTT-effect is created during welding and a stress free sample could not be provided. In literature no standard value is known for the materials analysed in this paper. Still, for calculation the lattice parameter at room temperature are taken from powder diffraction files (PDF). For the γ-phase the value $a_{0,\gamma} = 3.5911$ Å from the PDF 00-033-0397 for CrNi-steel and for the α-phase $a_{0,\alpha} = 2.8884$ Å from PDF 00–006–0696 for α-iron martensite are taken. Even if the calculated values are not reliable, they do still provide information about the course of the strains. The results cannot be evaluated quantitatively, but still a qualitative statement is possible. For this reason, the strain curves are shown without values.

First, the steady-state measurements of channel 0 (horizontal detector) are examined, Fig. 8. The curves show the strain profile of the

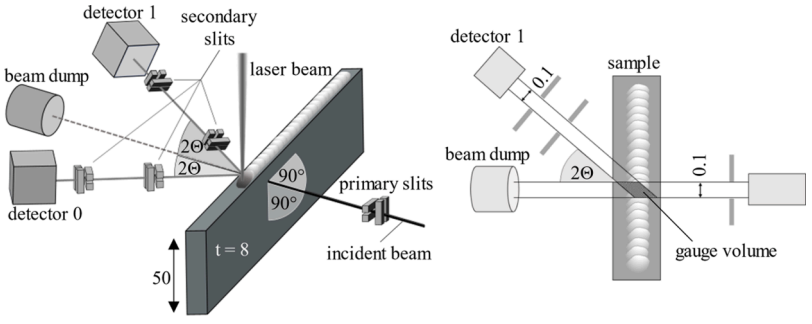

Fig. 3. EDXRD setup in the beamline P61A at DESY. Left: irradiated weld sample and the detectors. Right: Top view of the setup showing the gauge volume of the transmissive measuring method.

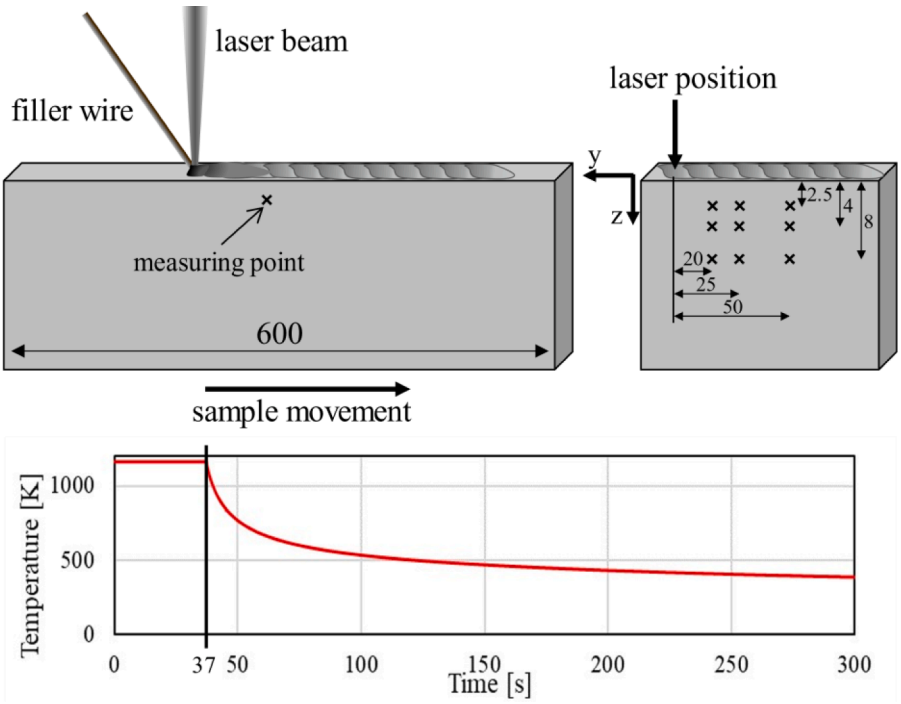

Fig. 4. Steady-state measurement during welding up to 37 s. The transient measurement starts after the welding finishes and the cooling of the sample takes place. For a better overview, the cooling in this figure is shown only up to 300 s. The magnification shows the individual measuring points.

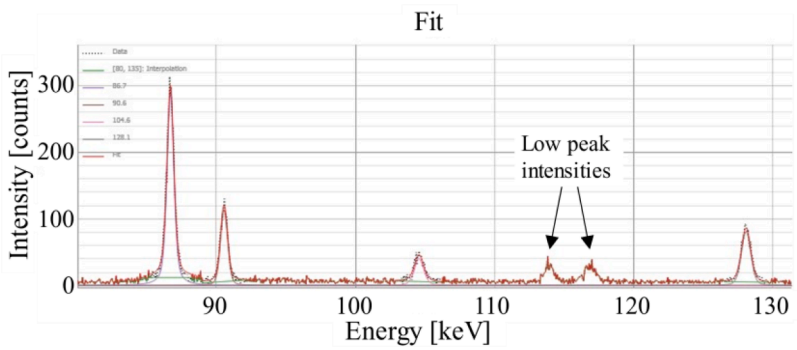

Fig. 5. Example of a peak fit from channel 0 showing some peaks that cannot be calculated by the program due to low peak intensity.

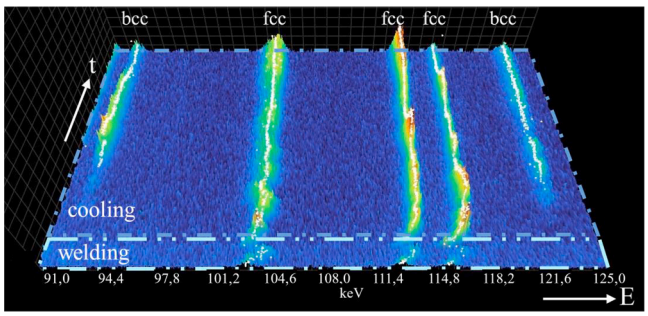

Fig. 6. Density Plot showing the welding cycle (steady-state measurement) and the cooling cycle (transient measurement) in the energy range of 91 keV to 125 keV for the complete measuring time of 500 s.

austenitic phase for the similar and dissimilar (LTT) welded samples. In this time period no ferrite is present in any sample. As mentioned, the strain in this time section is recorded over the weld length at isothermal state (steady-state measurement).

At a distance to the component surface of 2.5 mm the recording is close to the top of the weld. At a distance to the laser of −50 mm the strain curve in the LTT sample is relatively constant from start to finish. At a distance to the laser of −25 mm, however, the strain is shifted in the compression range and is not as constant. At −20 mm laser distance $\gamma_{\{311\}}$ could not be detected. In contrast, the similar welds show approximately the same strain curve at all distances to the laser and are overall more shifted in compressive strain range than the LTT samples.

The distance from the component surface of 4 mm is the position at the root of the weld seam. With LTT welds, the strain curves vary at all distances to the laser. Here, also, the strain curve at −50 mm is shifted to higher strain values. The lowest strain values (shift in compressive strain range) are present at a distance of −20 mm. For the similar welds the strain curves at -25 mm and -50 mm are close to each other and show lower strain values than the LTT samples. At −20 mm the lowest strain values (highest compressive strains) over all measuring points are present.

At a distance of 8 mm from the component surface, the measurements are taken from the base material. The strain curves at the individual measuring positions of the LTT samples also vary visibly here. The highest strain values are again present at −50 mm and are nearly

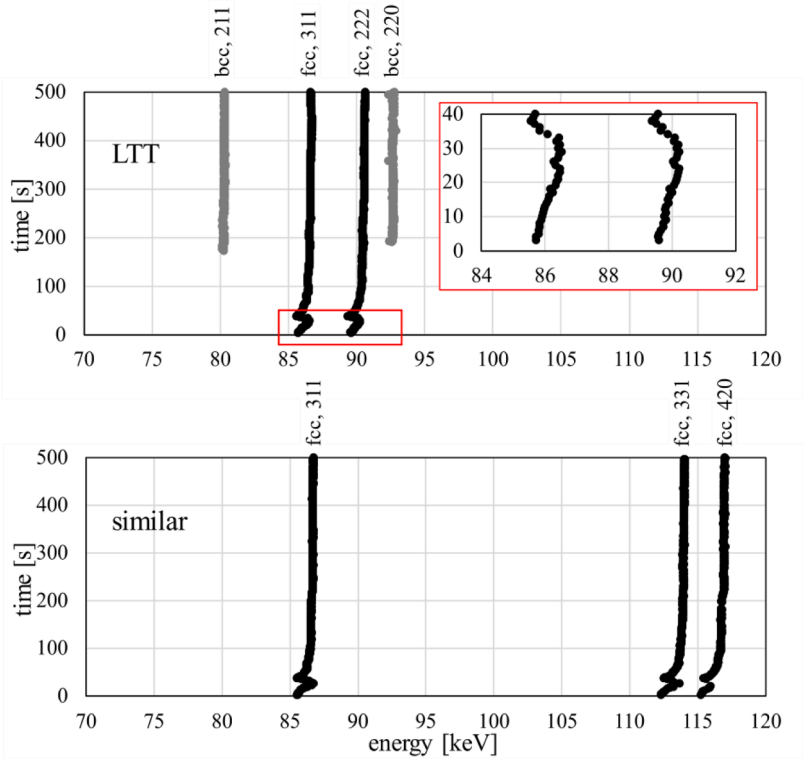

Fig. 7. Results of a sample at measuring point $z = 4$ mm and $y = -20$ mm in channel 0. Centre positions of the energy peaks showing the appearance of bcc-phase during cooling in the LTT-weld while in the similar weld only fcc-phase can be seen.

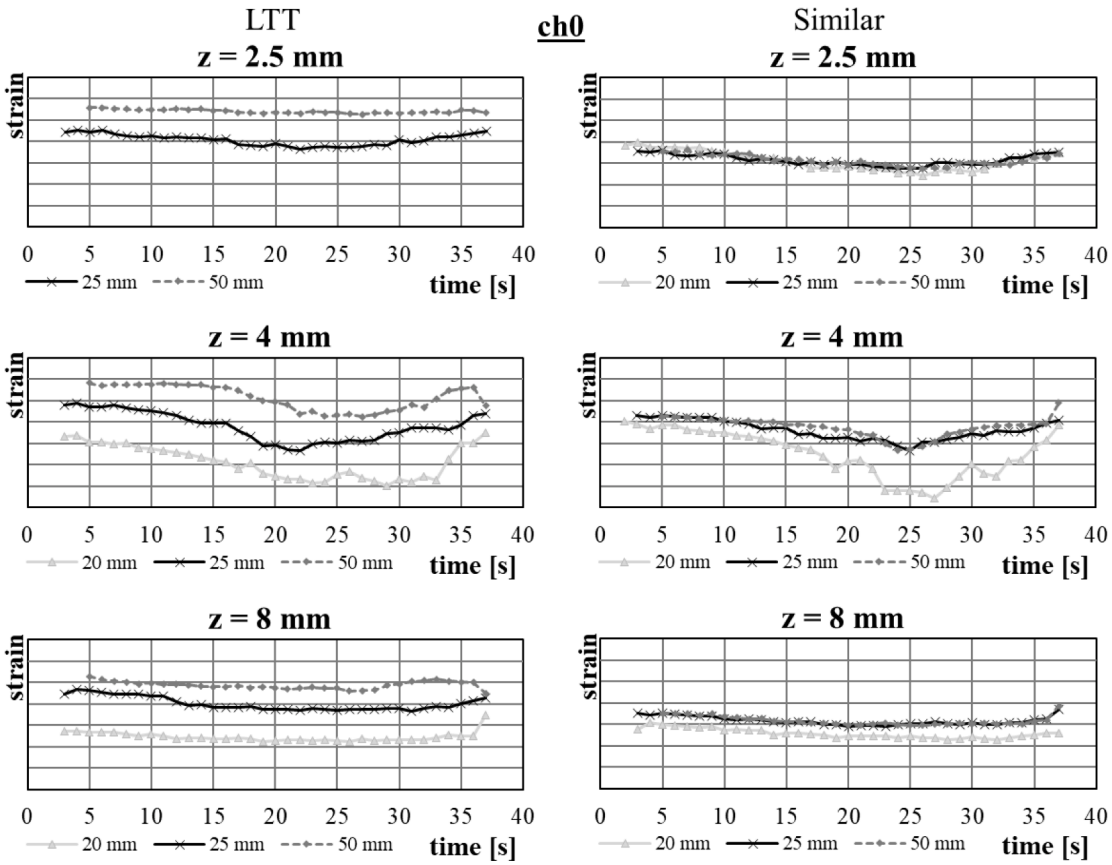

Fig. 8. Qualitative progression of strains during steady-state measurement (welding cycle) in channel 0 (horizontal detector). Graphs on the left show the strain progression for the dissimilar welded samples (LTT) and on the right side the strain progression of the similar welded samples.

constant. The lowest strains are present at a distance of −20 mm from the laser. For the similar welds, the strain curves are comparable to one another, with the curve for −20 mm being slightly lower strain range.

The strain curves tend to build up compressive strains and reduce towards the end of the welding time. At the beginning of the weld cycle the compressive strain is not high since most of the sample is not welded yet. During welding when reaching the middle of the sample, the compression strain increases, since the horizontal constriction of the surrounding material is high. When reaching the end of the sample, the compression reduces. This is due to differences in cooling rates in the middle and the end of the weld and the lack of constricting material close to the end.

Overall, in the LTT welds the measuring points further away from the weld seam show higher strain values in contrast to the measuring points close to the weld seam. In contrast, in the similar welds the strain values at −20 mm and −25 mm are close to each other. Only the strain values at −20 mm are lower at surface distances 4 mm and 8 mm. The lowest strains values can be found at a measuring depth of 4 mm (i.e. at the root of the weld) and −20 mm laser distance for both material combinations. The fact that the strains at 4 mm distance are lower than the other measuring positions is related to the fact that compression near the root of the weld is higher than in the upper region of the weld. In the root of a weld, more restrictions of the surrounding cold material are present. In comparison, the top of the weld seam can expand and contract more freely. Furthermore, it can be seen from the HAZ that the isotherms are closer together in the root area than in the outer areas. The differences in thermal expansions result in higher compression zones.

Generally, the strain curves of the LTT welds show higher discrepancies than the similar welds. These discrepancies are most likely due to the variations in chemical composition. As the chromium and nickel content in the LTT welds are reduced, the material properties and its response to thermal stress are altered. The expansion coefficients as well as the phase-specific stiffness change, and consequently different strain curves can be observed. For example, a study on Ni-CrC has shown that nickel experiences larger lattice strains because it has a lower stiffness (He et al., 2021). With a reduction of the nickel content less overall lattice strain can be a result. Since the thermal strain close to the weld is higher than with greater distance to the weld, higher absolute values can be observed at small distances to the laser. In the areas of high temperature, thermal shrinkage has a significant effect on the strain evolution, which is why the areas closer to the weld have higher compressive strain values than the measuring points further away. The discrepancy between the LTT strain curves in the root of the weld seam also affects the strain curves at a surface distance of 8 mm.

Next, the strains in channel 1 (vertical detector) are analysed, Fig. 9. In this channel, almost no difference can be seen between the LTT and similar welds. In all measuring points, slightly lower strains form in the middle of the sample and decrease towards the end of the weld. The vertical constriction of the sample is constant from beginning to the end (50 mm sample height) and the variation in strain values is due to the fact, that thermal distortion occurs. Here too, lower strains are present at −20 mm than at -50 mm. In contrast to channel 0, no high compressive strains (low strain values) are observed in the root of the weld seam. Furthermore, the LTT samples do not show any high discrepancies between the various measuring points. The variance in chemical composition in the weld seam does not influence the vertical strain progression.

A further examination is the strain curve during cooling in channel 0, Fig. 10. In the LTT welds, martensite strains are recorded in the measuring positions 2.5 mm and 4 mm from the surface in addition to the strains of the austenite phase. The austenitic strains increase to higher values while cooling takes place (tensile strains occur). In contrast to the austenitic strains, the martensitic strains remain constant over the entire cooling process. This is because the martensitic phase transformation takes place without diffusion and therefore the distortion continues at the same extent until the finish temperature is reached. The martensitic strains are shifted to lower strain values (compression strain range) compared to the austenitic strains. At 4 mm surface distance a more significant increase in elongation can be seen in the similar welds compared to the LTT welds.

At the 4 mm surface distance, the austenitic strains also show an

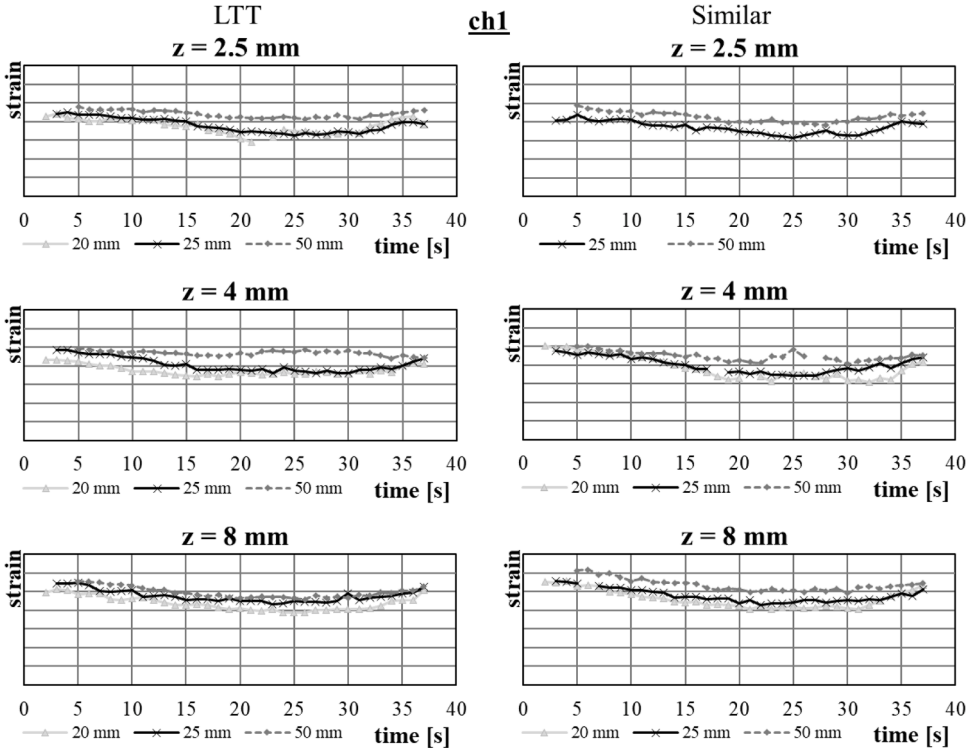

Fig. 9. Qualitative progression of strains during steady-state measurement (welding cycle) in channel 1 (vertical detector). Graphs on the left show the strain progression for the dissimilar welded samples (LTT) and on the right side the strain progression of the similar welded samples.

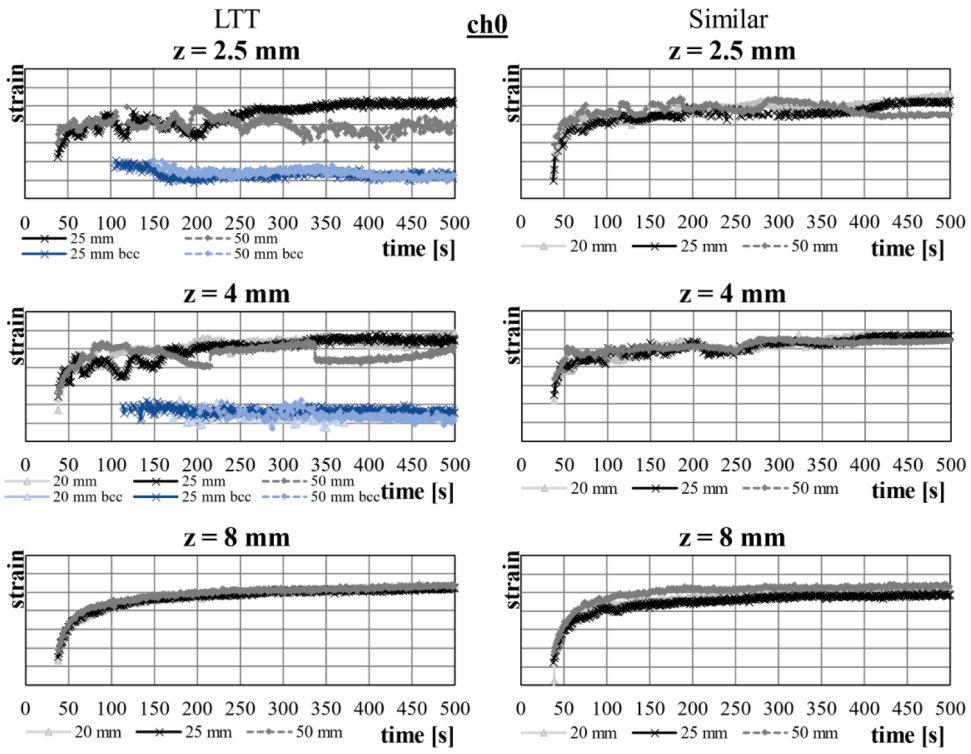

Fig. 10. Qualitative progression of strains during transient measurement (cooling cycle) in channel 0 (horizontal detector). Graphs on the left show the strain progression for the dissimilar welded samples (LTT) of austenite and martensite and on the right side the strain progression of the similar welded samples.

increase in strain. Here, the individual measuring points reach higher tensile values in a shorter amount of time for both the similar and the LTT welds compared to the row above. Compressive strains of the martensite phase are also constant from the beginning to the end of the cooling phase.

At a surface distance of 8 mm, the austenitic strains are comparable for both LTT and similar welds. Overall, a high strain increase can be observed here, which indicates the development of high tensile strains.

During the measurements in the steady-state phase, the highest compressive strains are found at a laser distance of −20 mm, while these

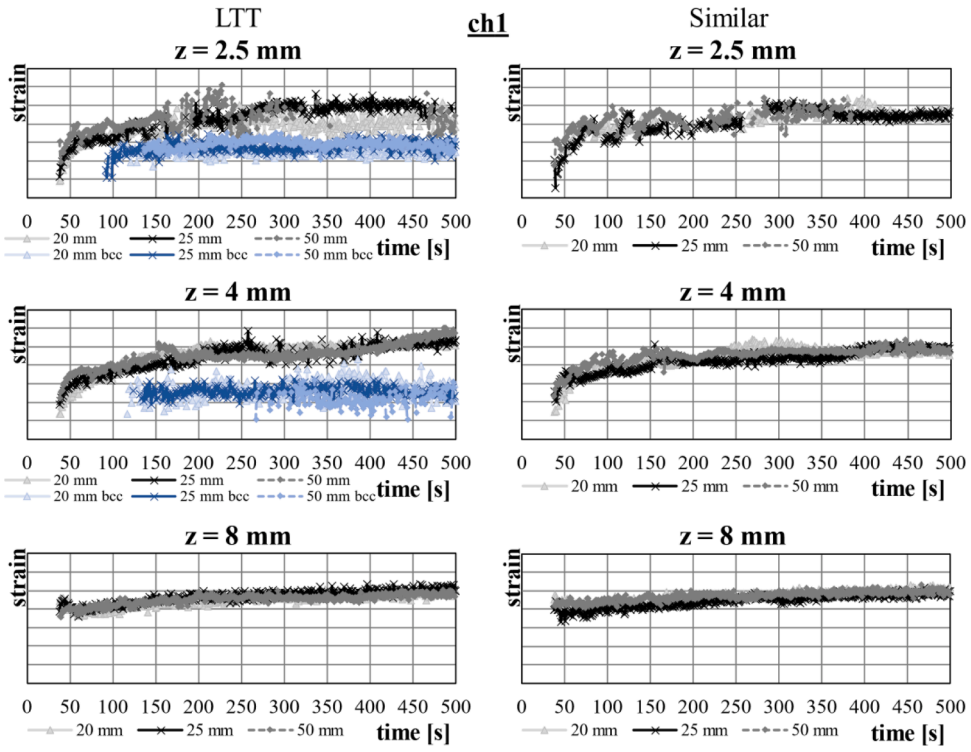

Fig. 11. Qualitative progression of strains during transient measurement (cooling cycle) in channel 1 (vertical detector). Graphs on the left show the strain progression for the dissimilar welded samples (LTT) of austenite and martensite and on the right side the strain progression of the similar welded samples.

were lowest at −50 mm. This tendency is not observed during the cooling phase. What is noticeable is that for all measurements in the weld seam (at z-distance 2.5 mm and 4 mm) the strain values fluctuate strongly while increasing. Inhomogeneities such as grain size distributions or chemical elements can lead to these fluctuations. In the base material, on the other hand, the strain in the austenitic material is generated purely by the thermal strain of the weld seam, which is why the increase occurs without major fluctuations.

Finally, the strains during cooling in channel 1 are analysed, Fig. 11. At a surface distance of 2.5 mm, the austenitic strains in the similar and LTT welds increase with no significant differences between the laser distances. What is noticeable is that the strains of the martensite phase are shifted to lower strains, but not as strongly as in channel 0. The difference between the austenitic strain and the martensitic strains are not as prominent.

At a surface distance of 4 mm, the austenitic strains increase to higher strain values. Here too, the martensite strains are constant and are shifted towards compressive strains, whereby lower strain values are present than in the row above. The difference between the austenitic strains and the martensitic strains are a bit more prominent.

The austenitic strain curves at 8 mm surface distance are different than the rows above or the strains in channel 0. Here, during cooling, the tensile strains still increase but not as much as any other measuring point and the curves are flatter. The difference in strain between the beginning and the end of the cooling phase is not as big. With the thermal shrinkage taking place, at this surface distance the strain is not affected in vertical direction, as it is affected in horizontal direction.

To understand how much strain is build up, the strain difference between the first and last time step of the cooling $\Delta\varepsilon_{trans}$ is calculated for the austenitic phase. This does allow to understand how much strain is occurring and delivers a quantitative assessment even if the previously calculated strain values are not accurate, Fig. 12.

In channel 0 looking into the similar welds it can be stated that the strain difference is higher than for the LTT welds. At 8 mm surface distance, the strain difference at -20 mm is highest. This means in this measuring position high tensile strains are built up. However, it is interesting to observe that at this measurement depth, the difference at -25 mm and -50 mm laser distance is much less and are almost the same. Apart from this anomaly, it can be noted that with increased distance to the laser, the difference $\Delta\varepsilon_{trans}$ decreases. As lower temperatures are present at greater distances, the strain changes become smaller. This trend is also true for the LTT welds. The strain differences for 8 mm surface distance are highest and are at -25 mm and -50 mm close to each other. At 2.5 mm surface distance the difference is the lowest. This means in the upper part of the LTT welds less tensile strains are build up than in the similar welds. The smallest change can be recorded at a laser distance of -50 mm with 2.5 mm surface distance for the LTT weld. Overall, in channel 0 the strain difference is on average highest at 8 mm surface distance for both LTT and similar welds, whereby the smallest differences are present in the LTT welds. A decrease in the difference indicates that more and more compressive strains are build up at greater distances to the laser.

In channel 1, however, the trend is reversed. The strain difference in 8 mm distance to the surface show the smallest values in both similar and LTT welds. In this channel, the values of $\Delta\varepsilon_{trans}$ do not change much for the different measuring positions. In the measuring positions -25 mm and -50 mm the values are close to each other for all surface distances with the only exception of the LTT weld at 2.5 mm surface distance and -50 mm laser distance. Here, the value decreases to lower values than the similar weld. All in all, it can be said that the values that are high in channel 0 are low in channel 1 and vice versa. The strain values that are low in the horizontal direction are compensated for in the vertical direction and increase as a result. The strains shift in direction so that the compressive strains build up in one direction can be compensated with the tensile strains in the other direction.

Conclusion

In this study, the comparison of similar and dissimilar welds in austenitic stainless steel base material to use the LTT effect shows the influence of the chemical composition and phase transformation on the strain evolution.

For the steady-state measurements in horizontal direction (channel 0) the lowest strain values are detected close to the middle of the weld where highest restrictions from the surrounding material is present. For both, similar and LTT welds the lowest strain values are reached at 4 mm surface distance with −20 mm laser distance, whereby the similar weld reaches lower values. Since at 4 mm the measuring position is close to the root of the weld, lower strain values are to be expected. Within the measuring points of the similar welds the strain curves do not vary much

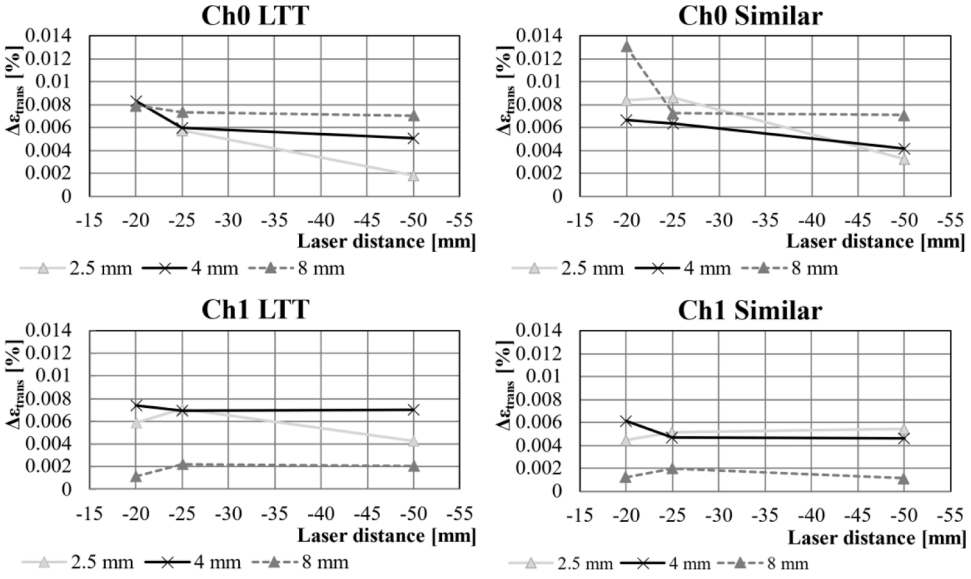

Fig. 12. Relationship between the strain difference $\Delta\varepsilon_{trans}$ and the measuring points in the transient measurement phase for LTT and similar welds in channel 0 (horizontal detector) and channel 1 (vertical detector). The value describes the difference between the strain values at the beginning and the end of the transient phase.

in between each other. For the LTT welds, on the other hand, a difference in the curves can be seen. Especially at 2.5 mm surface distance the strain values at −50 mm laser distance are nearly constant and show the highest strain values. In vertical direction (channel 1), however, the strains do not vary much between similar and LTT welds in any measuring position. The different chemical compositions do not influence the vertical strains.

During cooling, the dissimilar material combination implements low strains from martensite formation. In channel 0 the martensitic strains are shifted to lower strain values (compression) than in channel 1. Interesting to note is, that at 8 mm surface distance (base material) the strain increases during cooling in channel 0 (tensile strains are build up) while in channel 1 the strain curve is flat. Here, the tensile strains do not build up as prominent. The martensite formed in the LTT welds implement compression during the rest of the cooling cycle and affects the austenite strain in channel 0 but does not have an effect on the strains in channel 1.

Overall, the similar welds show lower strain values in the steady-state phase and reach higher strain values when cooled compared to the LTT welds in channel 0. With this knowledge it can be stated that the change in chemical composition and the LTT effect do have an influence on the strain evolution in horizontal direction by building up compressive strains. For the vertical direction, however, the comparison of strain progression of similar and LTT welds do not show much of a difference. The LTT effect has thus only an influence in horizontal or welding direction.

CRediT authorship contribution statement

F Akyel: Writing – review & editing, Writing – original draft, Visualization, Methodology, Investigation, Formal analysis, Data curation, Conceptualization. **M Gamerdinger:** Visualization, Investigation. **K Mäde:** Investigation. **K.R.Krishna Murthy:** Investigation. **S. Olschok:** Project administration, Funding acquisition. **R. Sharma:** Project administration. **U. Reisgen:** Project administration, Funding acquisition. **G. Abreu-Faria:** Methodology, Investigation, Conceptualization. **G. Dovzhenko:** .

Declaration of competing interest

The authors declare that they have no known competing financial interests or personal relationships that could have appeared to influence the work reported in this paper.

Data availability

Data will be made available on request.

Acknowledgement

The presented investigations were carried out at RWTH Aachen University Welding and Joining Institute ISF within the framework of the Collaborative Research Centre SFB1120-236616214 “Bauteilpräzision durch Beherrschung von Schmelze und Erstarrung in Produktionsprozessen” and funded by the Deutsche Forschungsgemeinschaft e.V. (DFG, German Research Foundation). The sponsorship and support is gratefully acknowledged.

We acknowledge DESY (Hamburg, Germany), a member of the Helmholtz Association HGF, for the provision of experimental facilities. Parts of this research were carried out at PETRA III and we would like to thank all staff members for assistance in using beamline P61A. Beamtime was allocated for proposal I-20210328.

References

Akyel, F., et al., 2022a. Adjustment of chemical composition with dissimilar filler wire in 1.4301 austenitic stainless steel to influence residual stress in laser beam welds. J. Adv. Join.Process. 5, 100081.

Akyel, F., et al., 2022b. Residual stress reduction with the LTT effect in low carbon manganese-steel through chemical composition manipulation using dissimilar filler material in laser beam welding. Metals 12 (6), 911. https://doi.org/10.3390/met12060911.

Altenkirch, J., et al., 2011. Time- and temperature-resolved synchrotron X-ray diffraction: observation of phase transformation and strain evolution in novel low temperature transformation weld filler materials. J. Strain. Anal. Eng. Des. 46 (7), 563–579. https://doi.org/10.1177/0309324711413190.

Azizpour, K., et al., 2019. Application of low transformation-temperature filler to reduce the residual stresses in welded component. JMES 13 (1), 4536–4557. https://doi.org/10.15282/jmes.13.1.2019.14.0384.

Bhadeshia, H.K.D.H., 2002. Handbook of Residual Stress and Deformation of Steel. ASM International.

Bhadeshia, H.K.D.H., Honeycombe, Robert William Kerr, 2017. Steels. Microstructure and Properties, 4th edition. Elsevier Butterworth-Heinemann, Amsterdam, Boston, Heidelberg, London, New York, Oxford, Paris, San Diego, San Francisco, Singapore, Sydney, Tokyo. ISBN: 9780081002728.

Bleck, W. (Ed.), 2016. Werkstoffkunde Stahl für Studium Und Praxis. RWTH Aachen. 6. überarb. Aufl.

Bühler, H., et al., 1933. Zusammenwirken von Wärme- und Umwandlungsspannungen in abgeschreckten Stählen. Archiv für das Eisenhüttenwesen 6 (7), 283–288. https://doi.org/10.1002/srin.193300417.

Francis, J.A., et al., 2007. Welding residual stresses in ferritic power plant steels. Mater. Sci. Technol. 23 (9), 1009–1020. https://doi.org/10.1179/174328407X213116.

Francis, J.A., Stone, H.J., Kundu, S., Rogge, R.B., Bhadeshia, H.K.D.H., Withers, P.J., Karlsson, L., 2008. Transformation temperatures and welding residual stresses in ferritic steels. In: Lidbury, D (Ed.), Proceedings of the ASME Pressure Vessels and Piping Conference - 2007: Presented at 2007 ASME Pressure Vessels and Piping Conference, July 22 - 26, 2007, San Antonio, Texas, USA. ASME, New York, NY, pp. 949–956.

Genzel, Ch., et al., 2011. Exploiting the features of energy-dispersive synchrotron diffraction for advanced residual stress and texture analysis. J. Strain. Anal. Eng. Des. 46 (7), 615–625. https://doi.org/10.1177/0309324711403824.

Gibmeier, J., et al., 2014. Real time monitoring of phase transformation and strain evolution in LTT weld filler material using EDXRD. J. Mater. Process. Technol. 214 (11), 2739–2747. https://doi.org/10.1016/j.jmatprotec.2014.06.008.

Giessen, B.C., et al., 1968. X-ray diffraction: new high-speed technique based on X-ray spectrography. Science 159 (3818), 973–975. https://doi.org/10.1126/science.159.3818.973.b.

He, L., et al., 2021. Synchrotron X-ray diffraction studies of the phase-specific deformation in additively manufactured Ni–CrC composites. Compos. Part B: Eng. 222, 109086 https://doi.org/10.1016/j.compositesb.2021.109086.

Igwemezie, Victor, et al., 2022. A review of LTT welding alloys for structural steels: design, application and results. J. Adv. Join. Process. 5, 100110 https://doi.org/10.1016/j.jajp.2022.100110.

Jenkins, R., Snyder, R.L., 1996. Introduction to X-ray Powder Diffractometry. Wiley, New York. https://doi.org/10.1002/9781118520994. Chemical analysis, V. 138.

Jones, W.K.C., et al., 1977. A model for stress accumulation in steels during welding. Metals Technol. 11, 557–566. Available online at. https://cir.nii.ac.jp/crid/1573105976091468416.

Klassen, Jakob, et al., 2017. Influence of residual stresses on fatigue strength of large-scale welded assembly joints. Weld. World 61 (2), 361–374. https://doi.org/10.1007/s40194-016-0407-8.

Kromm, A., et al., 2011. Characterizing PHASE TRANSFORMATIONS of different LTT alloys and their effect on RESIDUAL STRESSES and COLD CRACKING. Weld. World 55 (3–4), 48–56. https://doi.org/10.1007/BF03321286.

Kromm, A., Böllinghaus, Th., 2011. Umwandlungsverhalten und Eigenspannungen beim Schweißen neuartiger LTT-Zusatzwerkstoffe. Zugl.: magdeburg, Univ., Fak. für Maschinenbau, Diss., 2011. Berlin: Bundesanstalt für Materialforschung und -prüfung (BAM) (BAM-Dissertationsreihe, 72). ISBN: 978-3-9813853-9-7.

Laine, E., et al., 1980. The energy dispersive X-ray diffraction method: annotated bibliography 1968–78. J. Mater. Sci. 15 (2), 269–277. https://doi.org/10.1007/BF02396775.

Mikami, Y., et al., 2009. Angular distortion of fillet welded T joint using low transformation temperature welding wire. Sci. Technol. Weld. Join. 14 (2), 97–105. https://doi.org/10.1179/136217108X382972.

Mitter, W., 1987. Umwandlungsplastizität und ihre Berücksichtigung bei der Berechnung von Eigenspannungen. Mit 3 Tabellen. Berlin: Borntraeger (Materialkundlich-technische Reihe, 7). ISBN: 3-443-23008-3.

Ohta, A., et al., 1999. Fatigue strength improvement by using newly developed low transformation temperature welding material. Weld World 43, 38–42.

Ohta, A., et al., 2001. Fatigue. Fatigue strength improvement of lap joints of thin steel plates for automobile use by using low transformation temperature welding material. J. Soc. Mater. Sci. Jpn. 50 (10), 1086–1090. https://doi.org/10.2472/jsms.50.1086.

Ohta, A., et al., 2003. Fatigue strength improvement of lap welded joints by low transformation temperature welding wire — superior improvement with strength of steel. Weld. World 47 (3–4), 38–43. https://doi.org/10.1007/BF03266382.

Spieß, L., Teichert, Gerd, Schwarzer, Robert, Behnken, Herfried, Genzel, Christoph, 2009. Moderne Röntgenbeugung. Röntgendiffraktometrie für Materialwissenschaftler,

Physiker und Chemiker. 2., überarb. Und erw. Aufl. Vieweg + Teubner (Studium), Wiesbaden. https://doi.org/10.1007/978-3-8349-9434-9.
Wang, W., et al., 2002. New developed welding electrode for improving the fatigue strength of welded joints. J. Mater. Sci. Technol. 18 (6), 527–531.
Withers, P.J., et al., 2001. Residual stress. Part 2 – Nature and origins. Mater. Sci. Technol. 17 (4), 366–375. https://doi.org/10.1179/026708301101510087.
Wohlfahrt, H., et al., 1977. Die Ursachen des Schweißeigenspannungszustandes. Mater. Test. 19 (8), 272–280. https://doi.org/10.1515/mt-1977-190802.
Wohlfahrt, H., 1986. Die Bedeutung der Austenitumwandlung für die Eigenspannungsentstehung beim Schweißen. Härterei Technische Mittelungen 41 (5), 248–257.